Measurement of electron-attachment line shapes, cross sections, and rate constants in HI and DI at ultralow electron energies

S. H. Alajajian and A. Chutjian
Jet Propulsion Laboratory, California Institute of Technology, Pasadena, California 91109
(Received 21 September 1987)

Electron-attachment cross sections are reported in the electron energy range 0–150 meV, at an energy resolution of 6.5 meV (full width at half maximum) for the molecules HI and DI. Use is made of the Kr photoionization method to obtain cross sections for HI, and a signal intercomparison technique to obtain cross sections and the thermal-attachment rate constant for DI. Attachment properties of the two molecules are very similar. The ratio of attachment cross sections is discussed in terms of the reduced-mass dependence of the dissociation width and the survival probability, and in terms of spectroscopic thresholds and rotational populations for attachment at 300 K. Approximate potential-energy curves for the lowest states of the neutral molecule and negative ion are given.

I. INTRODUCTION

There has been considerable interest recently in the electron-attachment properties of molecules at extremely low electron energies. Mean energies $\bar{\varepsilon}$ below about 50 meV (580 K) correspond to the operating temperature of plasma devices such as a swarm plasma, gaseous dielectric, diffuse-discharge switch, and cooler regions of flames and exhausts. When one also considers that attachment cross sections for many molecules are *s* wave in nature (infinite cross section at threshold)[1,2] then one may have extremely large attachment rate constants at room temperature. This is observed for a large class of perfluorinated molecules, chlorofluorocarbon compounds SF_6, F_2, etc.

In this paper we report the first electron-attachment line shapes and cross sections for the diatomic molecules HI and DI at electron energies ε in the range $0 \leq \varepsilon \leq 150$ meV. We also report the first attachment rate constant at DI. As in previous studies with F_2 and other molecules,[3] the high resolution of the present work (6.5 meV, FWHM) using the krypton photoionization technique has revealed resolution-limited structure at threshold (zero electron energy). This phenomenon is again interpreted here in terms of a crossing, at zero energy, of the HI^- (or DI^-) ground-state potential energy curve with the ground-state neutral curve.

The krypton photoionization technique and the signal intercomparison method used in the present measurements are discussed in Sec. II. Results and interpretations in terms of a crossing between ground-state potential energy curves are given in Sec. III and conclusions are presented in Sec. IV.

II. EXPERIMENTAL METHODS

The general experimental approach uses the krypton photoionization method[1] to obtain attachment line shapes and cross sections for I^- formation from HI (abbreviated as I^-/HI). The intercomparison technique[4] is then used to compare the signal rate for I^-/DI with I^-/HI at the same electron energy ε. Measurement of the attachment line shape for I^-/DI then gives the attachment cross section for I^-/DI. Since this is the only dissociative channel open at thermal electron energies, integration of this attachment cross section with a Maxwellian electron energy distribution function (EEDF) gives an attachment rate constant at each mean energy $\bar{\varepsilon}$.

A. The krypton photoionization method

The krypton photoionization method is described in detail in Chutjian and Alajajian.[1] Briefly, krypton gas is photoionized at threshold, generating low-energy electrons of energy width determined by the slit width of the vacuum-ultraviolet monochromator. The electrons attach *in situ,* under single-collision conditions, to a small amount of the admixed target, and the appropriate negative ion is extracted from the collision region as a function of the photoionization wavelength (i.e., the electron energy).

The ionization of krypton atoms to the $^2P_{1/2}$ state by the step

$$\hbar\omega + \mathrm{Kr}(^1S_0) \rightarrow \mathrm{Kr}^+(^2P_{1/2}) + e(\varepsilon) \tag{1a}$$

produces electrons $e(\varepsilon)$ of energy ε, where ε is the difference between the photon energy $\hbar\omega$ and the photoionization threshold of Kr (14.666 eV), i.e., $\varepsilon = \hbar\omega - 14.666$ eV. The electrons attach in a field-free region to the admixed target gas (say, DI) to produce a negative ion (I^-), or

$$e(\varepsilon) + \mathrm{DI} \rightarrow \mathrm{D} + \mathrm{I}^- \ . \tag{1b}$$

Energetic electrons from the lower-lying $^2P_{3/2}$ onset do not play a role in the attachment process. These electrons have an energy of 0.67 eV at the $^2P_{1/2}$ threshold, and hence are too energetic to attach. Also, effects of collisional ionization of the *ns'* and *nd'* Rydberg levels converging to the $^2P_{1/2}$ limit are also not present, due to their rapid autoionization rate (order 10^{14} sec^{-1}), and as

evidenced by the sharp threshold onsets in the attachment line shapes.

We report herein attachment line shapes and cross section for the channels I^-/HI and I^-/DI. These line shapes are shown in Fig. 1 at a resolution of 6.5 meV (FWHM). Conditions of krypton and target pressures, data-accumulation times, electron energy range, and resolution $\Delta\varepsilon$ were similar to those of previous studies. In addition, special provisions were made in the case of HI and DI. The collision cell, quadrupole mass analyzer, and gas lines were baked for 24 h at 120 °C to remove any adsorbed water. Hydrogen iodide was then admitted, and the apparatus "passivated" over 24 h. The passivation was monitored by measuring the I^- signal rate. Measurements were begun when the signal had stabilized to better than 5% over 4 h. A total of three spectra each for HI and DI were obtained over a period of two weeks. As in previous studies, additional checks of the line shape at higher electron energies ($\varepsilon > 10$ meV) were carried out at larger slitwidths (and hence ion signal rates).

The attachment cross section is parametrized in the form

$$\sigma_A(\varepsilon)=N[a\varepsilon^{-1/2}\exp(-\varepsilon^2/\lambda^2)+\exp(-\varepsilon/\gamma)] , \quad (2)$$

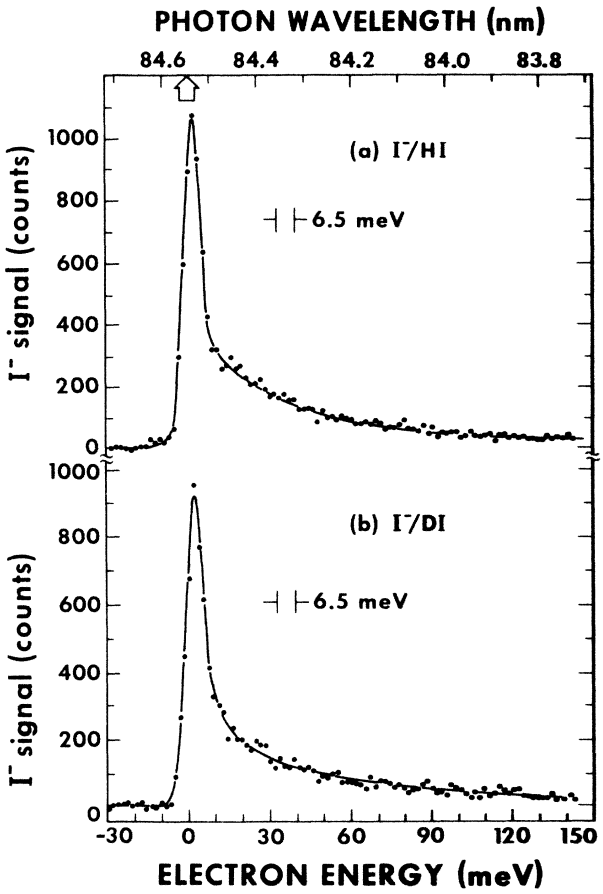

FIG. 1. Electron-attachment line shapes for the processes $e+HI(DI)\rightarrow H+I^-(D^-)$ at the indicated electron energy resolutions. Solid lines are computed fits to the experimental data. Arrow on top scale indicates threshold for ionization to the $^2P_{1/2}$ level of Kr^+ at 84.542 nm.

where the parameters a and λ are determined by a computed line fit with the experimental data (Fig. 1), γ from the high-energy ($\varepsilon > 10$ meV) portion of the line shape, and N by normalization to the appropriate thermal-attachment rate constant at 300 K through the expression

$$k(\bar{\varepsilon})=(2/m)^{1/2}\int_0^\infty \sigma_A(\varepsilon)\varepsilon^{1/2}f(\varepsilon)d\varepsilon , \quad (3)$$

where m is the electron mass, $k(\bar{\varepsilon})$ is the thermal-attachment rate constant at mean electron energy $\bar{\varepsilon}=38.78$ meV (300 K) and $f(\varepsilon)$ is the Maxwellian EEDF at $\bar{\varepsilon}$.

Implicit in the use of Eq. (3) is the fact that the particular attachment or dissociative attachment channel as measured by $k(\bar{\varepsilon})$ (in swarm or flowing-afterglow experiments[5–7]) and $\sigma_A(\varepsilon)$ (present experiments) must be the same. Since the channels I^-/HI and I^-/DI are the only channels open at these low electron energies, this is the case here. Further discussions of this point can be found in Refs. 4 and 7.

B. The intercomparison technique

In the present case, one has the attachment cross section in HI from the line shape unfolding [Eq. (2)] and the normalization [Eq. (3)] steps. To obtain cross sections for DI, we obtain the line-shape parameters a, λ, and γ from the deconvolution procedure, and the normalization constant N by comparing I^- signal rates $R_{DI}(\varepsilon)$ and $R_{HI}(\varepsilon)$ at an energy ε. This ratio $\rho(\varepsilon)$ of signal rates can be written as [Eq. (5) of Ref. 4]

$$\rho(\varepsilon)\equiv\frac{R_{DI}(\varepsilon)}{R_{HI}(\varepsilon)}=\frac{\Phi^{(1)}(\varepsilon)P_{Kr}^{(1)}P_{DI}\sigma_A^{DI}(\varepsilon)}{\Phi^{(2)}(\varepsilon)P_{Kr}^{(2)}P_{HI}\sigma_A^{HI}(\varepsilon)} . \quad (4)$$

Here P_{Kr} and P_{HI},P_{DI} refer to pressures of krypton and target gases, respectively, in the collision chamber, $\Phi(\varepsilon)$ the flux of vacuum-ultraviolet photons ionizing the Kr, and $\sigma_A^{HI}(\varepsilon)$,$\sigma_A^{DI}(\varepsilon)$ the attachment cross sections. The indices (1) and (2) refer to values during measurements of the rates $R_{DI}(\varepsilon)$ and $R_{HI}(\varepsilon)$, respectively. In practice, the light flux $\Phi(\varepsilon)$ is constant to better than 1% during the measurement cycle, and individual pressures can be adjusted such that, to better than 5%, $P_{Kr}^{(1)}=P_{Kr}^{(2)}$ and $P_{HI}=P_{DI}$, so that the ratio $\rho(\varepsilon)$ is now

$$\rho(\varepsilon)=\frac{\sigma_A^{DI}}{\sigma_A^{HI}}(\varepsilon) . \quad (5)$$

The measurement sequence is then (a) measure line shapes for HI and DI, (b) unfold to get parameters a, λ, and γ, (c) obtain N for HI by normalization to an appropriate $k(\bar{\varepsilon})$ (from Ref. 6), (d) use signal intercomparison [Eqs. (4) and (5)] to obtain $\sigma_A^{DI}(\varepsilon)$ and N for DI, (e) integrate $\sigma_A^{HI}(\varepsilon)$ and $\sigma_A^{DI}(\varepsilon)$ to obtain $k(\bar{\varepsilon})$ for HI and DI, respectively.

TABLE I. Cross-section parameters a, λ, γ, and N for HI and DI. The attachment cross section is defined by Eq. (2) over the energy range $0 \leq \varepsilon \leq 150$ meV. Units of $k(\bar{\varepsilon})$ are cm^3/s.

Molecule	a ($eV^{1/2}$)	λ (eV)	γ (eV)	N (cm^2)	Error in $\sigma_A(\varepsilon)$ (%)[a] $\varepsilon \leq 10$ meV	$\varepsilon > 10$ meV	$k(\bar{\varepsilon})$
HI	0.142	5.17×10^{-3}	6.29×10^{-2}	5.11×10^{-14}	18	15	$(3.0\pm0.9)\times10^{-7}$ [b]
DI	0.139	5.42×10^{-3}	5.57×10^{-2}	4.09×10^{-14}	20	17	$(2.2\pm0.8)\times10^{-7}$ [c]

[a]Listed error refers to smaller error limits in Fig. 2. Including error of $k(\bar{\varepsilon})$ (HI) from Ref. 6 gives a total error in $\sigma_A(\varepsilon)$ of 35%, shown as larger error limits in Fig. 2.
[b]From Ref. 6.
[c]Present results.

III. RESULTS AND DISCUSSION

Results of the computed fits to the line-shape data are shown as solid lines through the experimental points in Fig. 1. Values of a, λ, γ, and N are summarized in Table I. A value of

$$k(\bar{\varepsilon}) = (3.0\pm0.09)\times10^{-7}\ cm^3/s\ ,$$

from flowing-afterglow, Langmuir-probe (FALP) measurements[6] was used to obtain $\sigma_A(\varepsilon)$ for HI.

Values of N and $k(\bar{\varepsilon})$ for DI were obtained from measurements of $\rho(\varepsilon)$ at $\varepsilon = 20$, 40, and 60 meV. These values were 0.717, 0.726, and 0.766, respectively, to give an average value of

$$N = (4.09\pm0.31)\times10^{-14}\ cm^2\ .$$

Results for $\sigma_A^{HI}(\varepsilon)$ and $\sigma_A^{DI}(\varepsilon)$ are plotted in Fig. 2, along with the maximum s-wave capture cross section defined as

$$\pi\lambda^2\ (\text{in } cm^2) = 1.197\times10^{-12}\varepsilon^{-1}$$

(ε in meV). Also shown are data for HI and DI from a combined electron swarm-beam study.[8] These results were obtained at the lower energy limit of the swarm technique and could be considered to be in good agreement with present results. Electron-attachment rate constants are displayed in Fig. 3. As was found in previous calculations,[9,10] the effect on the calculated $k(\bar{\varepsilon})$ of a changing Boltzmann population of the target with $\bar{\varepsilon}$ was assumed to be negligible, i.e., the dominant process is attachment from a room-temperature (300 K) population (but see below).

One finds, as expected, very similar spectra, attachment cross sections, and rate constants for HI and DI. The magnitude of $\sigma_A(\varepsilon)$ for DI is uniformly lower by a factor 0.80 ± 0.09 relative to HI (the ratio of the values of N in Table I). To understand this, at least in part, it is helpful to examine the theoretical expression for the attachment cross section[9,11]

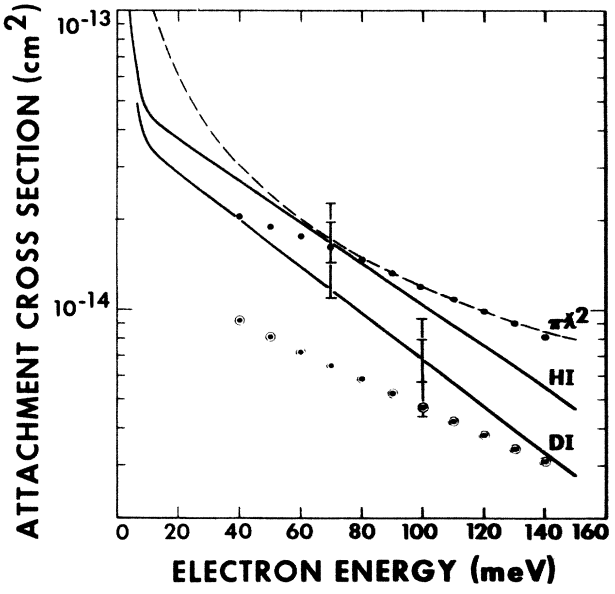

FIG. 2. Dissociative attachment cross sections for HI and DI in the electron energy range 0–150 meV. Cross sections for DI are obtained by intercomparing signals I^-/HI and I^-/DI. Smaller error limits refer to errors added in quadrature of present line shape and intercomparison measurements. Larger error limits are these errors added in quadrature with the error in $k(\bar{\varepsilon})$ (Ref. 6). Other results are swarm-beam unfolded values for HI (●●●) and DI (⊙⊙⊙) as read approximately from Fig. 3 of Ref. 8. The maximum s-wave capture cross section ($\pi\lambda^2$) is shown.

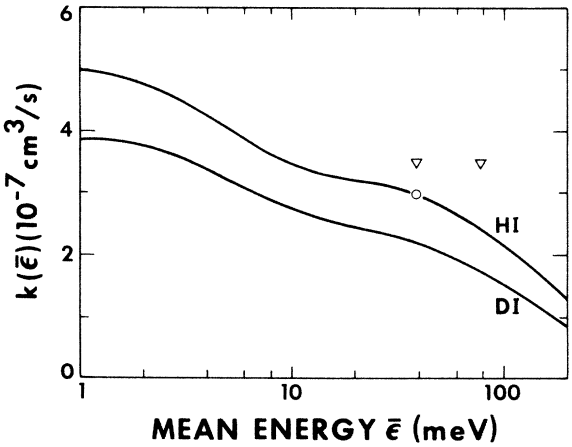

FIG. 3. Thermal-attachment rate constants $k(\bar{\varepsilon})$ with mean electron energy $\bar{\varepsilon}$. Present data for $\sigma_A(\varepsilon)$ are integrated with a Maxwellian electron energy distribution function, and refer to a room-temperature (300 K) v,J population. Triangles and circle are FALP results of Refs. 5 and 6, respectively.

$$\sigma_A(\varepsilon)=(4\pi^2 g/k^2)[\Gamma_a(\varepsilon)/\Gamma_d(\varepsilon)] \times |\tilde{\chi}(r_\varepsilon - i\Gamma_a/\Gamma_d)|^2 e^{-\rho(\varepsilon)} , \quad (6)$$

where k is the electron momentum ($\hbar^2k^2=2m\varepsilon$), $\Gamma_a(\varepsilon)$ and $\Gamma_d(\varepsilon)$ are the autoionization and dissociation widths, respectively, g is a spin-degeneracy factor (taken as 2), and r_ε is the turning point in the final state at energy ε. The quantity $\tilde{\chi}$ is the complex overlap integral between a vibrational level in the $X\,^1\Sigma^+$ ground electronic state and levels in the $X\,^2\Sigma^+$ ground state of HI^- or DI^-. The quantity $\rho(\varepsilon)$ is just twice the imaginary part of the complex final-state phase shift and $\exp[-\rho(\varepsilon)]$ the survival probability with $\rho(\varepsilon)$ given by

$$\rho(\varepsilon)=\int_{r_\varepsilon}^{r_c}\frac{\Gamma_a(\varepsilon)dr}{\hbar v(r)} . \quad (7)$$

Here, $v(r)$ is the classical reduced-mass velocity of the I^- and H (or D) particles, and r_c the crossing point between the neutral- and negative-ion states.

Mass dependence in Eq. (6) arises from several sources. (a) The heavier-reduced-mass (μ) particle will leave the Franck-Condon region more slowly, so that its dissociation width will be smaller. This dependence enters the cross section as $\mu^{1/4}$. (b) Because of its lower velocity, the larger μ will have a larger ρ [Eq. (7)], and the cross section will be correspondingly smaller for DI than for HI. The effect of (a) is trivial to calculate, and gives $\sigma_A^{DI}(\varepsilon)/\sigma_A^{HI}(\varepsilon)=1.19$. This is larger than the value of 0.80 observed here experimentally, and a value 0.69 of an energy-integrated cross-section ratio obtained in an electron-swarm study.[8] The effect of (b) is more difficult to assess. If ρ is much less than unity, as we have found in SF_6, $CFCl_3$, and CCl_4,[9,10] then the isotope effect will be negligible. If ρ is large, then its effect on the cross section will be significant, with a mass dependence, arising through the velocity in Eq. (7), given by $\rho\sim\mu^{1/2}$. Unfortunately, no information is available on the shape of the HI^- or DI^- $X\,^2\Sigma^+$ potential-energy curves, so that calculation of the magnitude of ρ is not possible. However, one could presume that a shallow well depth for the HI^- (DI^-) curve (see below) would give a small value of $v(r)$, or large value of ρ, and hence a significant mass dependence such that $\sigma_A^{HI}(\varepsilon)>\sigma_A^{DI}(\varepsilon)$.

Yet another interpretation of the smaller DI cross sections is possible, in light of the fact that the dissociation energy D_0^0 of DI appears to be known to better than 2 meV.[12] We show in Fig. 4 reasonable (Lennard-Jones) representations of the potential-energy curves for HI and HI^-. The $X\,^1\Sigma^+$ state of HI is described by an equilibrium internuclear distance r_e of 1.609 Å and a well depth $D_0^0=3.054\pm0.001$ eV. Corresponding values for DI are $r_e=1.609$ Å and $D_0^0=3.095\pm0.001$ eV.[12–14] The first excited state $1\Omega_{1/2}$ of HI^- is given by the experimental results of Le Coat, Azria, and Tronc.[15] No experimental or theoretical information is available on the ground state of HI^-, which has the molecular-orbital configuration

$$KLMN_{spd}(5s\sigma)^2(5p\sigma)^2(5p\pi)^4 6s\sigma .$$

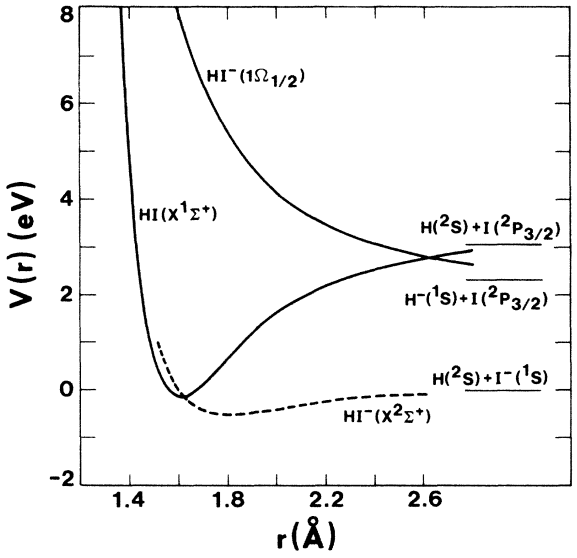

FIG. 4. Approximate set of potential energy curves for the lowest states of HI and HI^-. The potential energy curve for HI ($X\,^1\Sigma^+$) is drawn as a Lennard-Jones (6,12) potential, with $D_0^0=3.054$ eV and $r_e=1.609$ Å (Refs. 12–14); curve for $HI^-(1\Omega_{1/2})$ is from Ref. 15; while that for $HI^-(^2\Sigma^+)$ is an approximation, based on an assumed D_e of $\sim$0.5 eV and $r_e\sim1.8$ Å. The electron affinity of I is taken as 3.061 eV (Ref. 17).

Since the first available molecular orbital is a weakly antibonding $6s\sigma$ orbital, one would expect the HI^- state to be slightly bound or dissociative, and of $^2\Sigma^+$ symmetry.[16]

From spectroscopic data, onsets for attachment in HI(X) and DI(X) lie at energies $D_0^0-E_A(\mathrm{I})$, where $E_A(\mathrm{I})$ is the electron affinity of the iodine atom [3.061 eV (Ref. 17)]. These onsets are -0.007 eV for HI, and $+0.034$ eV for DI.[18] Hence, thermal attachment (300 K) to HI is exothermic, while that for DI is endothermic from the vibration-rotation levels $v=0$, $J=0$. Attachment becomes exothermic in DI for $J>8$, levels which lie above the level of maximum population $J_{max}=5$. Thus, the smaller cross sections in DI may also arise from the fact that the population fraction in $J\leq8$ is below threshold, and hence not available for attachment. This result would imply a large temperature dependence in $\sigma_A(\varepsilon)$ for DI. Especially if one cools the target such that population in $J>8$ is negligible, one should be able to "turn off" the attachment. This experiment is currently being planned in our laboratory.

IV. CONCLUSIONS

Attachment line shapes and cross sections have been measured for the molecules HI and DI at thermal electron energies and the thermal-attachment rate constant

obtained for DI. Both molecules exhibit the sharp, resolution-limited threshold characteristic of *s*-wave attachment. Hydrogen iodide is found to attach more strongly than deuterium iodide, an effect arising either from a reduced nuclear-mass dependence in the survival probability $e^{-\rho(\varepsilon)}$ or from the fact that a significant fraction of J levels at 300 K in DI lie below the threshold for attachment. Approximate potential-energy curves show that the HI^- and DI^- ground-state curves almost certainly have minima, and that the I^- fragment in both molecules leaves the attachment region with nearly zero kinetic energy.

ACKNOWLEDGMENTS

We are grateful to Dr. A. Temkin for several helpful discussions and correspondence during the course of this and previous research. Helpful discussions with Professor L. G. Christophorou and Dr. R. N. Compton are also acknowledged. This work was jointly sponsored by the Department of Energy and the National Science Foundation and was carried out at the Jet Propulsion Laboratory, California Institute of Technology, through agreement with the National Aeronautics and Space Administration.

[1]A. Chutjian and S. H. Alajajian, Phys. Rev. A **31**, 2885 (1985); S. H. Alajajian and A. Chutjian, J. Phys. B **19**, 2393 (1986).

[2]C. W. Walter, C. B. Johnson, A. Kalamarides, D. F. Gray, K. A. Smith, and F. B. Dunning, J. Phys. Chem. **91**, 4284 (1987).

[3]A. Chutjian and S. H. Alajajian, Phys. Rev. A **35**, 4512 (1987).

[4]S. H. Alajajian and A. Chutjian, J. Phys. B **20**, 2117 (1987).

[5]N. G. Adams, D. Smith, A. A. Viggiano, J. F. Paulson, and J. Henchman, J. Chem. Phys. **84**, 6728 (1986).

[6]D. Smith and N. G. Adams, J. Phys. B **20**, 4903 (1987).

[7]S. M. Spyrou, S. R. Hunter, and L. G. Christophorou, J. Chem. Phys. **83**, 641 (1985); S. R. Hunter and L. G. Christophorou, *ibid.* **80**, 6150 (1984).

[8]L. G. Christophorou, R. N. Compton, and H. W. Dickson, J. Chem. Phys. **48**, 1949 (1968). A better comparison would be between the energy-integrated cross section $\int_0^\infty \sigma_A(\varepsilon)d\varepsilon$ of the present work and that of Christophorou *et al.* This ratio is 0.73 (present) and 0.69 (Christophorou *et al.*). The actual integrated values of the present work are 4.23×10^{-15} cm^2 eV (HI) and 3.09×10^{-15} cm^2 eV (DI), as opposed to the values 3.72×10^{-15} and 2.56×10^{-15} for HI and DI, respectively, of Christophorou *et al.* (We have fixed the exponent of these last values from their Fig. 3, rather than from their Table I in which the exponents are obviously misprinted.)

[9]O. J. Orient and A. Chutjian, Phys. Rev. A **34**, 1841 (1986).

[10]O. J. Orient and A. Chutjian, *Abstracts of the Fifteenth International Conference on the Physics of Electronic and Atomic Collisions, Brighton, United Kingdom, 1987,* edited by J. Geddes, H. B. Gilbody, A. E. Kingston, C. J. Latimer, and H. J. R. Walters (Queens University, Belfast, 1987), p. 287.

[11]T. F. O'Malley, Phys. Rev. **150**, 14 (1966); **155**, 59 (1967).

[12]K. P. Huber and G. Herzberg, *Constants of Diatomic Molecules* (Van Nostrand-Reinhold, New York, 1979), pp. 325–326.

[13]H. J. Lempka, T. R. Passmore, and W. C. Price, Proc. R. Soc. London, Ser. A **304**, 53 (1968).

[14]D. A. Chapman, K. Balasubramanian, and S. H. Lin, Chem. Phys. Lett. **118**, 192 (1985).

[15]Y. Le Coat, R. Azria, and M. Tronc, J. Phys. B **18**, 809 (1985).

[16]M. Krauss and W. J. Stevens, J. Chem. Phys. **74**, 570 (1981).

[17]H. Hotop and W. C. Lineberger, J. Phys. Chem. Ref. Data **4**, 539 (1975).

[18]It appears that any potential-energy curve connecting the minimum of the neutral HI ground state, with the limit $H(^2S) + I^-(^1S)$, must have a minimum. For the sake of representation, we have shown this curve in Fig. 4 with a well depth of 0.50 eV, and an r_e of 1.80 Å. [See Krauss and Stevens (Ref. 16) for results of calculations in HCl^-, and D. Spence, W. A. Chupka, and C. M. Stevens, J. Chem. Phys. **76**, 2759 (1982) for detection of HI^-.] One also notes from Fig. 4 that the I^-, formed with extremely large cross section at thermal energies, must leave the collision region with essentially zero ion energy, making this system a potential high-brightness source for I^- ions.